Original Article

The value of morphological magnetic resonance imaging features combined with diffusion kurtosis imaging for predicting Ki-67 expression levels in high-grade gliomas

Ping Wang[1], Huan Huang[2], Lu Yang[1], Guangxiang Chen[1]

[1]Department of Radiology, the Affiliated Hospital of Southwest Medical University, Luzhou, China; [2]Department of MRI, the Affiliated Traditional Chinese Medicine Hospital of Southwest Medical University, Luzhou, China

Contributions: (I) Conception and design: P Wang, G Chen; (II) Administrative support: G Chen, L Yang; (III) Provision of study materials or patients: P Wang, H Huang; (IV) Collection and assembly of data: P Wang, H Huang, L Yang; (V) Data analysis and interpretation: P Wang, H Huang, L Yang; (VI) Manuscript writing: All authors; (VII) Final approval of manuscript: All authors.

Correspondence to: Guangxiang Chen, MD. Department of Radiology, the Affiliated Hospital of Southwest Medical University, No. 25 Taiping Street, Luzhou 646000, China. Email: cgx23ly2002@163.com.

Background: Accurate preoperative prediction of Ki-67 expression levels is especially crucial for developing appropriate individualized treatment plans and evaluating prognoses in patients with high-grade gliomas (HGGs). Although previous studies have shown that magnetic resonance imaging (MRI) can preoperatively predict Ki-67 expression levels in glioma, the optimal parameters and predictive performance remain controversial. In particular, there is insufficient research on the value of morphological MRI (mMRI) features and diffusion kurtosis imaging (DKI) for the preoperative assessment of Ki-67 expression levels in HGG. This study aimed to investigate the value of combining mMRI features with DKI for preoperative prediction of Ki-67 expression levels in HGG.

Methods: A total of 52 patients who were diagnosed with HGG by surgical pathology and who underwent conventional MRI and DKI scans were included in the study. The clinical and pathological characteristics, mMRI features, relative mean diffusivity (rMD), relative mean kurtosis (rMK), relative radial kurtosis (rKr), relative axial kurtosis (rKa), and relative fractional anisotropy (rFA) were compared between the Ki-67 high- and low-expression groups in HGG. Receiver operating characteristic (ROC) curves were plotted, and the areas under the curve (AUCs), as well as the sensitivities and specificities, were calculated. A nomogram for the prediction of Ki-67 expression levels in HGG was developed on the basis of the pivotal parameters from the mMRI and DKI. Calibration and decision curve analysis were used to evaluate the nomogram.

Results: The differences in tumor grade, subventricular involvement (SVI), boundary, diffusion restriction, enhancement, rMD, rMK, rKr, and rKa between the Ki-67 high- and low-expression groups in HGG were statistically significant ($P<0.05$). When the mMRI and DKI parameters were employed for individual diagnostics, the rMK exhibited the highest diagnostic efficiency, with an AUC value of 0.777 and a sensitivity and specificity of 80.0% and 67.6%, respectively. The diagnostic performance of the DKI model was superior to that of the mMRI model, with an AUC value of 0.834 and a sensitivity and specificity of 86.7% and 67.6%, respectively. The combination of the mMRI features and DKI yielded the optimal diagnostic performance, with an AUC value of 0.892 and a sensitivity and specificity of 100% and 67.6%, respectively. The C index for the nomogram was 0.874. The calibration and decision curve analysis confirmed that there was good consistency between the probability predicted by the nomogram and the actual probability and good clinical utility.

Conclusions: The combination of the mMRI and DKI is useful for noninvasive preoperative prediction of

HGG Ki-67 expression levels, and the nomogram may help in clinical decision-making for HGG patients.

Keywords: Glioma; Ki-67; magnetic resonance imaging (MRI); diffusion kurtosis imaging (DKI); nomogram

Submitted Sep 25, 2024. Accepted for publication Feb 19, 2025. Published online Mar 21, 2025.
doi: 10.21037/qims-24-2035
View this article at: https://dx.doi.org/10.21037/qims-24-2035

Introduction

High-grade gliomas (HGGs), which are classified as World Health Organization (WHO) grades 3 and 4, are prevalent primary malignant tumors of the central nervous system and represent approximately 25% of all adult central nervous system tumors (1-3). According to comprehensive treatment approaches, including safe tumor resection coupled with radiotherapy and chemotherapy, the overall prognosis for patients with HGG is still poor, with the median overall survival (OS) ranging from 9 to 12 months (4,5). Therefore, it is particularly important for HGG patients to adopt individualized treatment plans to maximize their progression-free survival (PFS) and OS as much as possible.

Ki-67 is a molecular marker of cell proliferation that is intimately linked to mitosis and can indicate the proliferative activity of tumor cells. The Ki-67 labelling index (LI) is closely correlated with tumor invasiveness, metastasis potential, and recurrence risk, providing a foundation for the development of personalized treatment plans and the assessment of patient prognosis (4,6-8). Studies have shown that the Ki-67 LI is closely associated with the survival, prognosis, and recurrence rates of patients with gliomas (4,9-12). Varlet *et al.* (10) reported that the Ki-67 LI served as an independent biomarker for OS in HGG patients, with a 10% increase in the Ki-67 LI correlated with a hazard ratio of 1.53. Kang *et al.* (4) reported that HGG patients with a high Ki-67 LI experienced a notably reduced 1-year PFS compared with those with a low Ki-67 LI and were more susceptible to recurrence. Kumar Suman *et al.* (12) reported that the Ki-67 LI was negatively correlated with survival time and that patients with a low Ki-67 LI experienced improved postoperative outcomes. At present, the quantification of Ki-67 requires the use of histopathological biopsy or surgical resection of the tumoral tissue. These methods, however, are not only invasive and expensive but also prone to sampling errors, limiting their widespread application before surgery (13). Consequently, accurate preoperative prediction of Ki-67 expression levels is crucial for patients with HGG.

Magnetic resonance imaging (MRI) is a widely utilized, convenient, and effective technique that can noninvasively provide both macroscopic and microscopic details of the entire brain tissue prior to surgery. Morphological MRI (mMRI) features, such as tumor location, number, boundary, and enhancement patterns, can be easily and quickly used to predict tumor grade, molecular classification, and the Ki-67 LI (13-15). However, the limitation is that these assessments are heavily susceptible to observer bias and lack quantifiability. The diffusion kurtosis imaging (DKI) model, which is based on the non-Gaussian distribution of water molecules, enables a quantitative assessment of the extent to which diffusion deviates from Gaussian behavior and reveals the constraints on water molecule diffusion and the complexity inherent in the structural composition of a tissue (16,17). Consequently, it facilitates the evaluation of the tumor microenvironment. Recent studies have indicated that DKI holds significant promise for predicting tumor grade, genotype, the Ki-67 LI, and patient prognosis (18-23). However, there remains a debate over the optimal parameters and the performance of these predictive models. To our knowledge, few studies have explored the preoperative predictive value of mMRI features and DKI for Ki-67 expression levels in HGG.

We aimed to investigate the value of the combination of mMRI features and DKI for preoperatively predicting Ki-67 expression levels in HGG. We hypothesized that the combination of these two techniques would more effectively assess Ki-67 expression levels in HGG patients and could provide a basis for the development of personalized treatment strategies and the assessment of patient prognosis in HGG patients. We present this article in accordance with the STARD reporting checklist (available at https://qims.amegroups.com/article/view/10.21037/qims-24-2035/rc).

Methods

Patients

In general, from January 2019 to December 2023, data

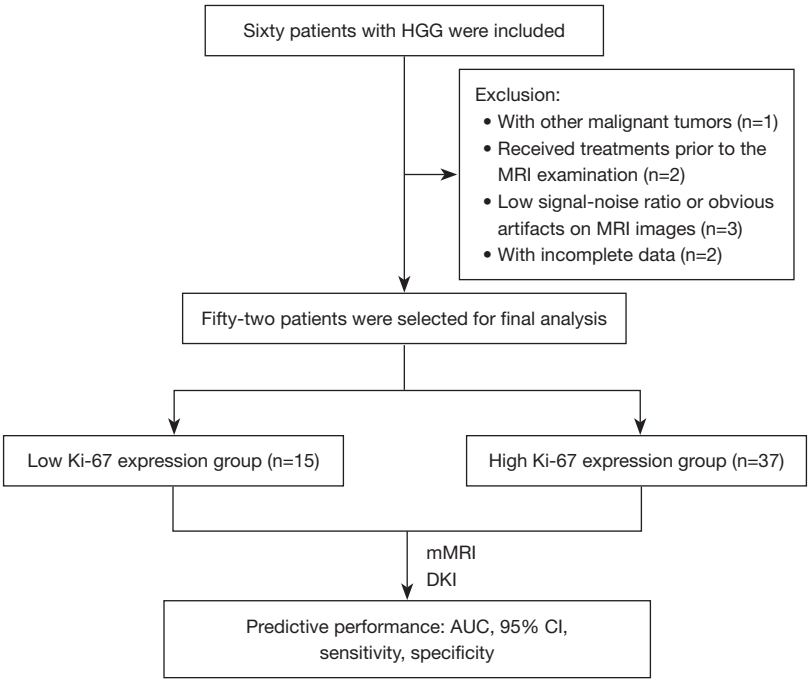

Figure 1 Flow diagram of patient recruitment. HGG, high-grade glioma; MRI, magnetic resonance imaging; mMRI, morphological magnetic resonance imaging; DKI, diffusion kurtosis imaging; AUC, area under the curve; CI, confidence interval.

from patients diagnosed with HGG confirmed by surgical pathology at the Affiliated Hospital of Southwest Medical University were collected prospectively and randomly. The inclusion criteria were as follows: (I) all patients had undergone plain MRI, DKI, and contrast-enhanced scans prior to surgery; (II) all patients had undergone surgical treatment and were pathologically confirmed to have HGG post-surgery; (III) all patients had undergone pathology and immunohistochemistry analysis post-surgery to ascertain the WHO tumor grade, the Ki-67 LI and isocitrate dehydrogenase (*IDH*) gene status; and (IV) all patients were aged 18 years older. The exclusion criteria were as follows: (I) patients diagnosed with other malignant tumors; (II) patients who had undergone surgery, radiotherapy, or other treatments prior to the MRI examination; (III) patients with a low signal-noise ratio or obvious artifacts on MRI images that compromised the observation; and (IV) patients with incomplete data. The detailed patient selection flow diagram is shown in *Figure 1*. A total of 52 patients were enrolled in the study. The study was conducted in accordance with the Declaration of Helsinki (as revised in 2013). This study was approved by the Ethics Committee of the Affiliated Hospital of Southwest Medical University (No. KY2023041), and informed consent was provided by all individual participants.

MRI data acquisition

All MR examinations were performed with a 3.0 T system and a 64-channel head-phased array coil (MAGNETOM Prisma, Siemens Healthineers, Erlangen, Germany). The scan sequences included T1-weighted imaging (T1WI), T2-weighted imaging (T2WI), fluid-attenuated inversion recovery (FLAIR), DKI, and contrast-enhanced T1WI. The main scan parameters were as follows: (I) T1WI: repetition time (TR) =200 ms, echo time (TE) =2.46 ms, slice thickness =5.0 mm, field of view (FOV) =22.0×22.0 cm^2, matrix =320×320; (II) T2WI: TR =4,090 ms, TE =109 ms, slice thickness =5.0 mm, FOV =22.0×22.0 cm^2, matrix =320×320; (III) FLAIR: TR =7,500 ms, TE =88 ms, inversion time =2,297.50 ms, slice thickness =5.0 mm, FOV =22.0×22.0 cm^2, matrix =256×256; (IV) DKI: TR =3,900 ms, TE =76 ms, slice thickness =5.0 mm, FOV =22.0×22.0 cm^2, matrix =128×128, b=0, 1,000, and 3,000 s/mm^2, with 30 gradient directions; and (V) contrast-enhanced T1WI: TR =250 ms, TE =2.5 ms, slice thickness =5.0 mm. Gadopentetate dimeglumine (Magenev, Bayer, Leverkusen, Germany) was administered intravenously via the cubital

vein at a flow rate of 1.0 mL/s and a dose of 0.1 mmol/kg of body weight.

Image analysis

Two radiologists (with 10 and 8 years of experience) performed a blinded evaluation of the mMRI features and quantified the DKI-derived parameters in patients diagnosed with HGG. Disagreements were resolved through consultation. The mMRI feature evaluation included the number of tumors (solitary or multiple), the degree of brain lobe involvement (single or multiple), subventricular involvement (SVI, presence or absence), cortical involvement (presence or absence), midline structure involvement (presence or absence), side (left or right), boundary (clear or unclear), necrosis (presence or absence), hemorrhage (presence or absence), cysts (presence or absence), diffusion restriction (presence or absence), peritumoral edema (presence or absence), enhancement (presence or absence), and major diameter of the tumor. SVI was defined as involvement within 5 mm of the lateral ventricular boundary on the enhanced scan (24,25). The cysts were well defined, exhibited a round or oval shape, and presented with regions of low signal intensity on T1WI and high signal intensity on T2WI, without evidence of enhancement (13). Diffusion restriction was defined as the presence of a high signal within the tumor on DKI images with a b value of 1,000 s/mm^2. Enhancement was defined as higher signal intensity on contrast-enhanced T1WI images than on T1WI images without contrast. The DKI images were imported into the Diffusional Kurtosis Estimator to generate pseudo color maps of the mean diffusivity (MD), mean kurtosis (MK), radial kurtosis (Kr), axial kurtosis (Ka) and fractional anisotropy (FA). With respect to the contrast-enhanced T1WI or T2WI images, the regions of interest (ROIs) were manually drawn in the tumor parenchyma and contralateral normal-appearing white matter, focusing on the largest section of the tumor's solid component on the pseudo color map and avoiding areas such as cystic degeneration, necrosis, calcification, and hemorrhage. At least three ROIs should be positioned, each with an area ranging from 30 to 40 mm^2. The mean values of the parameters obtained from DKI within the tumor parenchyma were normalized by dividing them by the corresponding values of the contralateral normal-appearing white matter, yielding the following normalized parameters: relative mean diffusivity (rMD), relative mean kurtosis (rMK), relative radial kurtosis (rKr), relative axial kurtosis (rKa), and relative fractional anisotropy (rFA). The mMRI features and DKI-derived parameter values were evaluated and measured in the same manner in all patients by a radiologist (with 10 years of experience) with at least a 1-month interval to evaluate intraobserver agreement.

Histology and immunohistochemistry

The surgical resection samples were subjected to pathological evaluation after being stained with hematoxylin and eosin and the Ki-67 LI was determined via immunohistochemistry with streptavidin-peroxidase conjugation. From each section, five fields were randomly chosen, and a total of 1,000 cells were tallied. When the nucleus exhibited brown-yellow coloration, it was considered positive. The Ki-67 LI was the ratio of positively stained cells to the overall count of cells examined. Patients were categorized into two groups on the basis of this index: those with high expression (Ki-67 >10%) and those with low expression (Ki-67 ≤10%) (9,26-28). *IDH1/2* mutations were detected by Sanger sequencing, and *IDH* mutation was diagnosed when a mutation was present in any one of them (20).

Statistical analysis

The software SPSS 27.0 (IBM Corp., Armonk, NY, USA) and R (4.2.1 version, http://www.R-project.org) were used for the statistical analysis. Cohen's kappa and intraclass correlation coefficient (ICC) analyses were performed on the data collected by the two observers. When the kappa coefficient and ICC value of inter- or intra-observer reliability exceeded 0.75, the consistency of the data was deemed good. The count data were represented by frequencies, and the intergroup comparisons were performed via the χ^2 test. The measurement data were represented as the means ± standard deviations. An independent samples *t*-test was used if the measurement data conformed to a normal distribution; otherwise, the Mann-Whitney *U* test was used. Statistically significant variables were included in the binary logistic regression analysis to establish prediction models. The receiver operating characteristic (ROC) curves for the Ki-67 expression levels predicted by both the mMRI and DKI were plotted. The nomogram, calibration curves, and decision curves for the pivotal parameters from the mMRI and DKI were plotted. The performance of the nomogram for the prediction of Ki-67 expression levels in HGG patients was assessed in the

Table 1 Clinical and pathological characteristics of participants

Characteristics	Low Ki-67 expression (n=15)	High Ki-67 expression (n=37)	t/χ^2 value	P value
Age (years)	46.20±8.56	51.14±15.37	t=–1.168	0.248
Gender			χ^2=1.626	0.202
Male	6 (40.0)	22 (59.5)		
Female	9 (60.0)	15 (40.5)		
Tumor grade			χ^2=17.173	<0.001
Grade 3	12 (80.0)	7 (18.9)		
Grade 4	3 (20.0)	30 (81.1)		
IDH			χ^2=2.193	0.139
Mutant	6 (40.0)	6 (16.2)		
Wild type	9 (60.0)	31 (83.8)		

Chi-squared test and independent samples *t*-test were used. Continuous variables were represented by mean ± standard deviation, and count data were represented by frequency (%). IDH, isocitrate dehydrogenase.

entire cohort. A P value <0.05 was regarded as statistically significant.

Results

Clinical and pathological characteristics of the participants

The clinical and pathological characteristics of the included glioma patients are summarized in *Table 1*. A significant difference in tumor grade was detected between the high and low Ki-67 expression groups in HGG (P<0.001), whereas no significant differences in age, gender, or *IDH* gene status were detected between the two groups (age, P=0.248; gender, P=0.202; *IDH*, P=0.139).

Consistency analysis of parameters

The kappa coefficients of inter- and intra-observer reliability for the number of HGG lesions, degree of brain lobe involvement, SVI, cortical involvement, midline structure involvement, side, boundary, necrosis, hemorrhage, cysts, diffusion restriction, peritumoral edema, and enhancement ranged from 0.853 to 0.961 and 0.812 to 0.961, respectively. The ICC values of inter- and intra-observer reliability for the major diameter, rMD, rMK, rKr, rKa and rFA ranged from 0.842 to 0.997 and 0.928 to 0.994, respectively. The inter- and intra-observer reliability of the mMRI features and DKI parameters was good, as shown in Tables S1,S2.

Comparison of the mMRI features of HGG patients with different Ki-67 expression levels

There were statistically significant differences in the SVI, boundary, diffusion restriction, and enhancement between the high and low Ki-67 expression groups in HGG (P<0.05), whereas there were no significant differences in the number of lesions, degree of brain lobe involvement, cortical involvement, midline structure involvement, side, necrosis, hemorrhage, cysts, peritumoral edema, or major diameter between the two groups (P>0.05), as shown in *Table 2* and *Figures 2,3*.

Comparison of the DKI parameters of HGG patients with different Ki-67 expression levels

The differences in rMD, rMK, rKr, and rKa between the high and low Ki-67 expression groups in HGG patients were statistically significant (P<0.05), whereas the difference in rFA between the two groups was not statistically significant (P>0.05), as shown in *Table 3*. Representative samples with different Ki-67 expression levels are shown in *Figures 2,3*.

Performance evaluation of parameters for predicting high and low Ki-67 expression in HGG patients

ROC curves of the mMRI features (SVI, boundary, diffusion restriction, and enhancement) and DKI parameters (rMD, rMK, rKr, and rKa), both individually and in combination,

Table 2 mMRI features comparison of the high and low Ki-67 expression groups in HGG

Parameters	Low Ki-67 expression (n=15)	High Ki-67 expression (n=37)	χ^2/Z value	P value
Number of lesions			χ^2=0.006	0.938
Solitary	13 (86.7)	30 (81.1)		
Multiple	2 (13.3)	7 (18.9)		
Degree of brain lobe involvement			χ^2=0.933	0.334
Single	7 (46.7)	12 (32.4)		
Multiple	8 (53.3)	25 (67.6)		
SVI			χ^2=6.048	0.014
Presence	5 (33.3)	26 (70.3)		
Absence	10 (66.7)	11 (29.7)		
Cortical involvement			χ^2=0.344	0.557
Presence	9 (60.0)	27 (73.0)		
Absence	6 (40.0)	10 (27.0)		
Midline structure involvement			χ^2=1.050	0.306
Presence	8 (53.3)	14 (37.8)		
Absence	7 (46.7)	23 (62.2)		
Side			χ^2=0.094	0.760
Left	7 (46.7)	19 (51.4)		
Right	8 (53.3)	18 (48.6)		
Boundary			χ^2=4.873	0.027
Clear	8 (53.3)	32 (86.5)		
Unclear	7 (46.7)	5 (13.5)		
Necrosis			χ^2=0.000	>0.99
Presence	13 (86.7)	31 (83.8)		
Absence	2 (13.3)	6 (16.2)		
Hemorrhage			χ^2=0.321	0.571
Presence	6 (40.0)	18 (48.6)		
Absence	9 (60.0)	19 (51.4)		
Cysts			χ^2=1.394	0.238
Presence	10 (66.7)	18 (48.6)		
Absence	5 (33.3)	19 (51.4)		
Diffusion restriction			χ^2=12.849	<0.001
Presence	7 (46.7)	35 (94.6)		
Absence	8 (53.3)	2 (5.4)		
Peritumoral edema			–	0.619
Presence	13 (86.7)	34 (91.9)		
Absence	2 (13.3)	3 (8.1)		
Enhancement			–	0.006
Presence	10 (66.7)	36 (97.3)		
Absence	5 (33.3)	1 (2.7)		
Major diameter (cm)	4.68±1.67	4.62±1.71	Z=−0.182	0.856

Chi-squared test and Mann-Whitney *U* test were used. Continuous variables were represented by mean ± standard deviation, and count data were represented by frequency (%). – represents Fisher's exact probability method. mMRI, morphological magnetic resonance imaging; HGG, high-grade glioma; SVI, subventricular involvement.

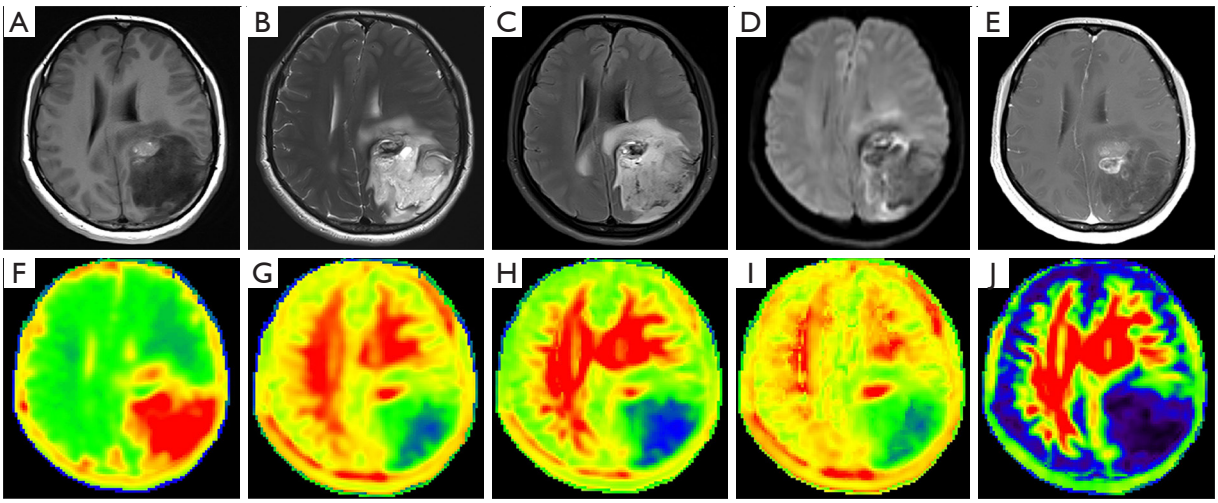

Figure 2 A 42-year-old female with HGG in the left parieto-occipital lobe (grade 3, Ki-67 =10%). (A) The mass is hypointense and nodular-like hyperintense on T1WI, with an unclear boundary. (B,C) The mass shows mixed signal intensities on T2WI and FLAIR, accompanied by peritumoral edema and involving the cortex. (D) The mass shows punctate and striated hyperintensity on DKI (b=1,000 s/mm^2). (E) Contrast-enhanced T1WI of the mass shows marked inhomogeneous enhancement. (F) MD map; (G) MK map; (H) Kr map; (I) Ka map; (J) FA map. HGG, high-grade glioma; T1WI, T1-weighted imaging; T2WI, T2-weighted imaging; FLAIR, fluid-attenuated inversion recovery; DKI, diffusion kurtosis imaging; MD, mean diffusivity; MK, mean kurtosis; Kr, radial kurtosis; Ka, axial kurtosis; FA, fractional anisotropy.

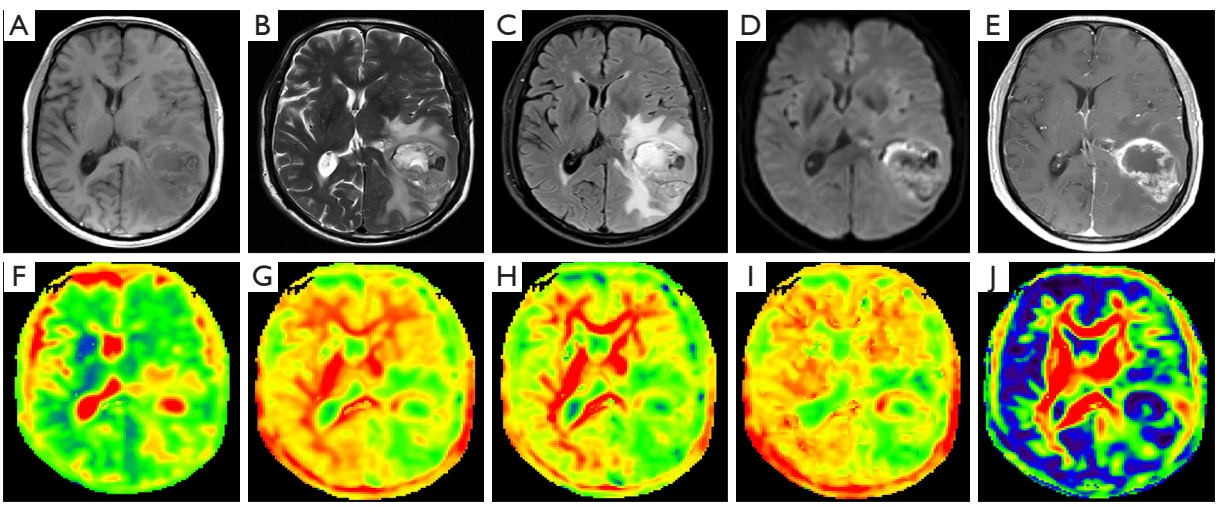

Figure 3 A 68-year-old male with HGG in the left temporal-parietal lobe (grade 4, Ki-67 =80%). (A) The mass shows mixed signal intensities on T1WI, with a clear boundary. (B,C) The mass shows high intensity and nodular-like hypointense on T2WI and FLAIR, accompanied by peritumoral edema and cortical involvement. (D) The mass shows inhomogeneous hyperintensity on DKI (b=1,000 s/mm^2). (E) Contrast-enhanced T1WI of the mass shows a marked enhancement rim, accompanied by SVI; (F) MD map; (G) MK map; (H) Kr map; (I) Ka map; (J) FA map. HGG, high-grade glioma; T1WI, T1-weighted imaging; T2WI, T2-weighted imaging; FLAIR, fluid-attenuated inversion recovery; DKI, diffusion kurtosis imaging; SVI, subventricular involvement; MD, mean diffusivity; MK, mean kurtosis; Kr, radial kurtosis; Ka, axial kurtosis; FA, fractional anisotropy.

Table 3 DKI parameters comparison of the high and low Ki-67 expression groups in HGG

Parameters	Low Ki-67 expression (n=15)	High Ki-67 expression (n=37)	*t*/Z value	P value
rMD	1.69±0.38	1.38±0.29	Z=−3.080	0.002
rMK	0.60±0.16	0.77±0.15	*t*=−3.677	<0.001
rKr	0.58±0.19	0.65±0.14	Z=−2.090	0.037
rKa	0.77±0.14	0.88±0.17	*t*=−2.202	0.032
rFA	0.37±0.22	0.43±0.24	Z=−1.060	0.289

Independent samples *t*-test and Mann-Whitney *U* test were used; continuous variables were represented by mean ± standard deviation. DKI, diffusion kurtosis imaging; HGG, high-grade glioma; rMD, relative mean diffusivity; rMK, relative mean kurtosis; rKr, relative radial kurtosis; rKa, relative axial kurtosis; rFA, relative fractional anisotropy.

Table 4 Diagnostic performance of mMRI features and DKI parameters for differentiating high and low Ki-67 expression groups in HGG

Parameters	Cut off	AUC	95% CI	Sensitivity	Specificity
SVI	–	0.685	0.540–0.829	0.667	0.703
Boundary	–	0.666	0.524–0.808	0.467	0.865
Diffusion restriction	–	0.740	0.604–0.875	0.553	0.946
Enhancement	–	0.653	0.527–0.779	0.333	0.973
mMRI	–	0.795	0.641–0.949	0.600	0.946
rMD	1.420	0.773	0.638–0.908	0.933	0.568
rMK	0.695	0.777	0.631–0.922	0.800	0.676
rKr	0.555	0.691	0.501–0.881	0.733	0.730
rKa	0.905	0.683	0.525–0.841	0.867	0.460
DKI	0.761	0.834	0.711–0.957	0.867	0.676
mMRI + DKI	0.882	0.892	0.804–0.979	1.000	0.676

mMRI, morphological magnetic resonance imaging; DKI, diffusion kurtosis imaging; HGG, high-grade glioma; SVI, subventricular involvement; rMD, relative mean diffusivity; rMK, relative mean kurtosis; rKr, relative radial kurtosis; rKa, relative axial kurtosis; AUC, area under the curve; CI, confidence interval.

predicting high and low Ki-67 expression levels in HGG patients are depicted in *Table 4* and *Figure 4A-4C*.

Development and performance of the Ki-67 expression nomogram

The nomogram, calibration curves, and decision curves based on the parameters with areas under the curve (AUCs) greater than 0.7 are shown in *Figure 5A-5C*. The concordance index (C-index) for the nomogram was 0.874. The calibration and decision curve analysis confirmed that there was good consistency between the probability predicted by the nomogram and the actual probability and good clinical utility. An optimal cut-off value of 140 points for the total points of the nomogram (corresponding to a hazard level of 0.5) was determined, and all patients were divided into high- and low-risk groups of Ki-67 expression according to the total points. The discrimination of the two groups was achieved in the entire cohort (P<0.001), as shown in *Table 5*. According to the risk classifier, the accuracy, sensitivity, and specificity of the nomogram in the entire cohort were 84.6%, 91.9%, and 66.7%, respectively.

Discussion

Ki-67 is a nuclear protein that is exclusively expressed in proliferating cells. The Ki-67 LI represents the proliferative activity of cells and serves as a critical factor in the

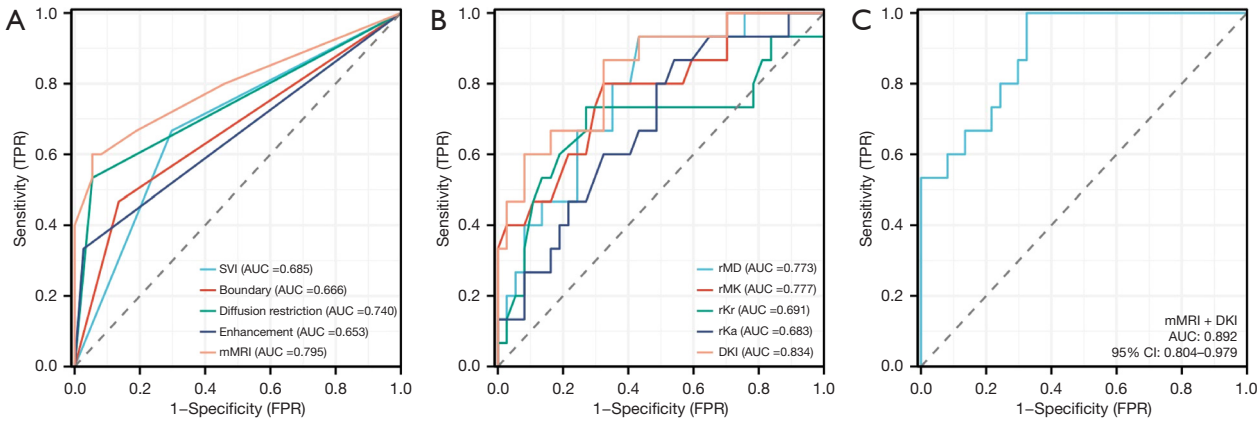

Figure 4 ROC curves for the prediction of Ki-67 expression levels in HGG. (A) ROC curves of the mMRI features; (B) ROC curves of the DKI parameters; (C) ROC curve of the combination of the mMRI features and DKI. TPR, true positive rate; FPR, false positive rate; SVI, subventricular involvement; AUC, area under the curve; mMRI, morphological magnetic resonance imaging; rMD, relative mean diffusivity; rMK, relative mean kurtosis; rKr, relative radial kurtosis; rKa, relative axial kurtosis; DKI, diffusion kurtosis imaging; CI, confidence interval; ROC, receiver operating characteristic; HGG, high-grade glioma.

determination of treatment regimens and evaluation of the prognosis of patients with HGG (7,8). MRI is helpful for noninvasive preoperative evaluation of the Ki-67 expression status in tumors (13-15,21). This study compared the clinical and pathological characteristics, mMRI features, and DKI-derived parameters of HGG patients with high and low Ki-67 expression levels. HGG patients with high Ki-67 expression were more likely to have a higher WHO grade than those with low expression. The mMRI features, including the SVI, boundary, diffusion restriction, and enhancement, exhibited significant differences between the high and low Ki-67 expression groups. Except for rFA, all derived parameters from DKI exhibited significant differences between the high and low Ki-67 expression groups. The combination of mMRI features and DKI demonstrated the highest predictive efficiency for Ki-67 expression levels in HGG. In summary, the mMRI features and DKI serve as valuable preoperative imaging biomarkers for distinguishing between high and low Ki-67 expression in HGG. To facilitate its clinical use, a diagnostic nomogram was developed on the basis of parameters with an AUC greater than 0.7, which can assist clinicians in formulating personalized treatment strategies and assessing the prognosis of patients with HGG before surgery.

At present, there is still much controversy about the cut-off values for high and low Ki-67 expression in tumors. Li *et al.* (9) and Torun *et al.* (29) adopted a 10% threshold to categorize Ki-67 expression levels, distinguishing between high expression (Ki-67 >10%) and low expression (Ki-67 ≤10%). They reported that glioma patients with high Ki-67 expression experienced shorter PFS and OS, a heightened risk of recurrence and mortality, and a less favorable prognosis (9). The current study also referenced this cut-off value.

The present study revealed that HGG patients with a high level of Ki-67 expression were more frequently associated with a higher WHO grade than were those with a low expression level, which was consistent with the findings of previous studies (9,30). Additionally, this study compared the mMRI features and DKI-derived parameters of high and low Ki-67 expression groups within HGG. The lesions in the high Ki-67 expression group presented more distinct boundaries and were more prone to diffusion restrictions, SVIs, and enhancements, which was partially consistent with the results reported by Yang *et al.* (13). The reasons are as follows: gliomas in the high Ki-67 expression group tend to have a higher pathological grade (30) and exhibit a relatively high degree of cell proliferation, increased cell density, and restricted diffusion of water molecules (28), which is more likely to result in a high signal on DKI images; gliomas with high Ki-67 expression are also characterized by a relatively high degree of malignancy and invasiveness, increasing the likelihood of invasion into surrounding anatomical structures, such as the subependymal region, which are closely associated with the survival outcomes of glioma patients (31,32); and tumors with high Ki-67 expression undergo rapid and invasive growth, accompanied by a substantial increase in tumor blood flow and pronounced disruption of the

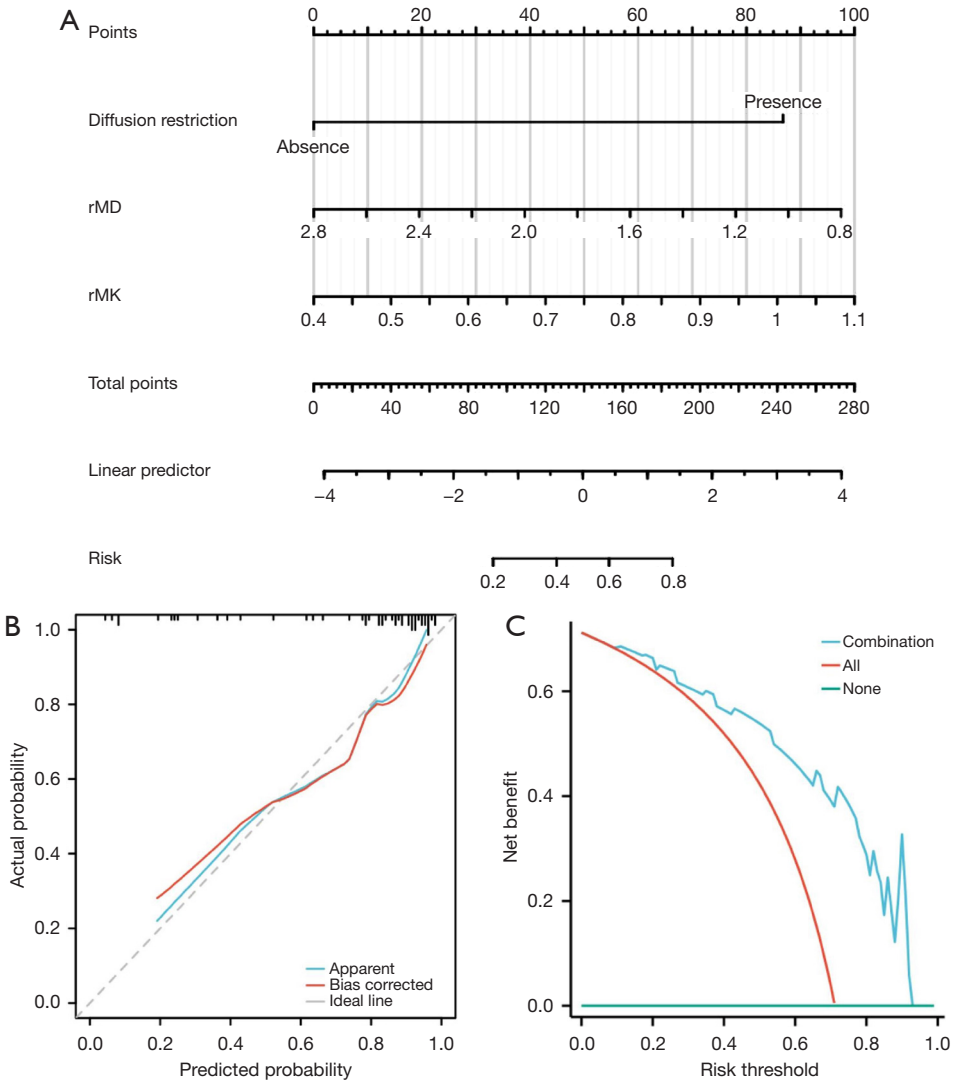

Figure 5 Nomogram, calibration curves, and decision curves for the prediction of Ki-67 expression levels in HGG. (A) Nomogram for the prediction of Ki-67 expression levels in HGG; (B) calibration curves for the prediction of Ki-67 expression levels in HGG; (C) decision curves for the prediction of Ki-67 expression levels in HGG. HGG, high-grade glioma; rMD, relative mean diffusivity; rMK, relative mean kurtosis.

Table 5 The risk-classification performance of nomogram

Risk of Ki-67 expression	High Ki-67 expression (n=37)	Low Ki-67 expression (n=15)	χ^2 value	P value
High risk	34	5	16.521	<0.001
Low risk	3	10		

blood-brain barrier (33,34), making them more susceptible to enhancement. In this study, no significant differences were observed in the tumor major diameter, intratumoral necrosis, or hemorrhage between the high and low Ki-67 expression groups in HGG, which was inconsistent with the results of Bai *et al.* (35). The following speculations have been made: initially, there was variation in the inclusion criteria. The current study included patients with WHO grade 3–4 HGG, whereas Bai *et al.* (35) specifically included patients with WHO grade 4 glioblastoma. Second, the evaluation criteria were distinct. Bai *et al.*'s (35) study concentrated on assessing the proportions of necrosis and hemorrhage, but this study exclusively investigated the presence of necrosis and hemorrhage. In this study, the rMD of the HGG high Ki-67 expression group was notably lower than that of the HGG low Ki-67 expression group, and the rMK, rKr, and rKa were significantly greater than those of the HGG low Ki-67 expression group, which aligns with the findings of Cui *et al.* (36), who utilized DKI to predict Ki-67 expression levels in rectal cancer patients. It is speculated that as the Ki-67 LI increases, tumor cell proliferation becomes more vigorous, cell density increases, and the arrangement becomes more compact, thereby restricting the diffusion of water molecules and leading to a reduction in the value of rMD (16,28); tumors with high Ki-67 expression tend to grow at a faster rate, often with inadequate blood supply, which results in significant ischemia and hypoxia within the tumor and causes increased intratumoral hemorrhage, necrosis, cystic degeneration, and a more intricate microstructure (3,34,37,38). Consequently, this leads to increases in the values of rMK, rKr, and rKa (16,37). However, studies have reported that the values of DKI-derived parameters are influenced by a variety of factors, including the choice of the b-value, the number of gradient directions, the selection of the ROI, signal-noise ratio, and artifacts (39-41). Notably, the optimal selection of the b-value and gradient direction remains a subject of debate (39-41), which may affect the reproducibility and generalizability of DKI in clinical practice. Therefore, standardizing the parameters for DKI scans is essential.

Currently, MRI has been employed in studies to preoperatively predict the Ki-67 expression level in glioma patients; however, the optimal parameters and predictive accuracy are still the subject of debate. Su *et al.* (42) employed the T2-FLAIR, apparent diffusion coefficient (ADC), MD, FA, and MK parameters to individually predict high and low Ki-67 expression levels in glioma. In their research, the AUC values for T2-FLAIR, ADC, MD, FA, and MK ranged from 0.750 to 0.865. Upon combining these parameters for joint prediction, the AUC value improved to 0.870. Zhu *et al.* (43) reported that the AUC values for predicting high and low Ki-67 expression in glioblastoma were 0.710 for contrast-enhanced T1WI, 0.830 for T2WI, and 0.760 for the ADC value within intratumoral areas. When these three parameters were combined, the AUC value increased to 0.900. In this study, when the mMRI and DKI parameters were independently used to predict high and low Ki-67 expression in HGG, the AUC value for the rMK parameter was the highest, which aligns with the findings of Zhang *et al.* (21), who employed DKI to predict Ki-67 expression levels in soft tissue sarcoma, suggesting that the rMK value may more accurately reflect the microscopic structure of tumors (21). In our study, when the rMK, rKr, and rKa values were greater than 0.695, 0.555, and 0.905, respectively, while the rMD was less than 1.420, there was a greater likelihood of HGG with high Ki-67 expression. However, the diagnostic accuracy of individual parameters is limited (AUC: 0.653–0.777), whereas the efficacy is enhanced when multiple parameters are used in combination (AUC: 0.795–0.892). Upon diagnosis with the mMRI (SVI, boundary, diffusion restriction, enhancement) and DKI (rMD, rMK, rKr, rKa) models, the AUC value of the DKI model exceeded that of the mMRI. It is speculated that DKI-derived parameters can be employed to quantitatively assess the diffusion of water molecules and the complexity and heterogeneity of the tissue structure in HGG, providing a more accurate reflection of the subtle alterations within the tumor microstructure (16,17), whereas mMRI features represent a qualitative visual assessment, which is susceptible to observer subjectivity and a lack of quantitative measures, potentially leading to reduced diagnostic accuracy. The AUC value reached its peak when the mMRI features were combined with DKI, indicating that the combination of qualitative data from the mMRI features and quantitative data from the DKI model could be employed to evaluate both the macroscopic and microscopic conditions of HGG in a more comprehensive manner, thereby more accurately predicting the Ki-67 expression level of HGG and enhancing diagnostic efficacy. Furthermore, an easy-to-use diagnostic nomogram was developed to assess Ki-67 expression levels in HGG patients in our study. The diagnostic nomogram achieved favorable predictive value in internal tests. Through the nomogram, clinicians can noninvasively predict the Ki-67 expression levels of HGG before surgery in routine clinical practice, and aid in developing personalized treatment

strategies and evaluating the prognosis of HGG patients. Considering the small sample size of HGG patients with low Ki-67 expression in this study, the representativeness of the general population may be insufficient, which could introduce bias into the predictive outcomes for HGG Ki-67 expression levels. The findings of this study necessitate further validation through an expansion of the sample size, which will constitute our subsequent research focus.

The limitations of this study are as follows: (I) this was a single-center study, and the sample size was relatively small, especially for patients with low Ki-67 expression in HGG. The ability of mMRI features combined with DKI for predicting Ki-67 expression levels in HGG should be further validated in a larger patient cohort. (II) Due to the high degree of heterogeneity in HGG, ROI-based measurements may not consistently reflect the Ki-67 LI in pathological samples. (III) HGG patients were not categorized on the basis of the *IDH* genotype, which may have had some impact on the results. (IV) The parameters for DKI scans have not yet been standardized. Future research will further explore these aspects.

Conclusions

The combination of mMRI features and DKI is helpful for the preoperative, noninvasive prediction of Ki-67 expression levels in HGG, and the diagnostic nomogram can offer valuable assistance in tailoring individualized treatments and evaluating the prognosis of patients with HGG in routine clinical practice.

Acknowledgments

None.

Footnote

Reporting Checklist: The authors have completed the STARD reporting checklist. Available at https://qims.amegroups.com/article/view/10.21037/qims-24-2035/rc

Funding: This work was supported by the Sichuan Science and Technology Program of China (grant No. 2022YFS0616) and the Project for Doctors of the Affiliated Hospital of Southwest Medical University (grant No. 2018-17129).

Conflicts of Interest: All authors have completed the ICMJE uniform disclosure form (available at https://qims.amegroups.com/article/view/10.21037/qims-24-2035/coif). The authors have no conflicts of interest to declare.

Ethical Statement: The authors are accountable for all aspects of the work in ensuring that questions related to the accuracy or integrity of any part of the work are appropriately investigated and resolved. The study was conducted in accordance with the Declaration of Helsinki (as revised in 2013). The study was approved by the Ethics Committee of the Affiliated Hospital of Southwest Medical University (No. KY2023041), and informed consent was provided by all individual participants.

References

1. Roustaei H, Vosoughi H, Askari E, Aziz Kalantari B, Norouzbeigi N, Anvari K, Beheshti M, Aryana K. [68 Ga] Ga-CXCR4 PET/CT imaging in high-grade glioma for assessment of CXCR4 receptor expression. Eur J Radiol 2024;180:111694.
2. Kowalczyk A, Zarychta J, Marszołek A, Zawitkowska J, Lejman M. Chimeric Antigen Receptor T Cell and Chimeric Antigen Receptor NK Cell Therapy in Pediatric and Adult High-Grade Glioma-Recent Advances. Cancers (Basel) 2024;16:623.
3. Berger TR, Wen PY, Lang-Orsini M, Chukwueke UN. World Health Organization 2021 Classification of Central Nervous System Tumors and Implications for Therapy for Adult-Type Gliomas: A Review. JAMA Oncol 2022;8:1493-501.
4. Kang HJ, Kim M, Kwak YK, Shin J, Lee SJ. Reduced volume intensity-modulated radiotherapy with simultaneous integrated boost for patients with high-grade glioma: A retrospective observational study. Medicine (Baltimore) 2023;102:e33955.
5. Yanchu L, Rong P, Rong C, Li Z, Xiaoyan Y, Feng W. Ozone therapy for high-grade glioma: an overview. Front

Oncol 2023;13:1161206.
6. Luo X, Zheng R, Zhang J, He J, Luo W, Jiang Z, Li Q. CT-based radiomics for predicting Ki-67 expression in lung cancer: a systematic review and meta-analysis. Front Oncol 2024;14:1329801.
7. Finkelman BS, Zhang H, Hicks DG, Turner BM. The Evolution of Ki-67 and Breast Carcinoma: Past Observations, Present Directions, and Future Considerations. Cancers (Basel) 2023;15:808.
8. Ni J, Zhang H, Yang Q, Fan X, Xu J, Sun J, Zhang J, Hu Y, Xiao Z, Zhao Y, Zhu H, Shi X, Feng W, Wang J, Wan C, Zhang X, Liu Y, You Y, Yu Y. Machine-Learning and Radiomics-Based Preoperative Prediction of Ki-67 Expression in Glioma Using MRI Data. Acad Radiol 2024;31:3397-405.
9. Li F, Wang D, Wang N, Wu L, Yu B. A nomogram with Ki-67 in the prediction of postoperative recurrence and death for glioma. Sci Rep 2024;14:20334.
10. Varlet P, Le Teuff G, Le Deley MC, Giangaspero F, Haberler C, Jacques TS, Figarella-Branger D, Pietsch T, Andreiuolo F, Deroulers C, Jaspan T, Jones C, Grill J. WHO grade has no prognostic value in the pediatric high-grade glioma included in the HERBY trial. Neuro Oncol 2020;22:116-27.
11. Kumar A, Das KK, Kanjilal S, Jain N, Mishra P, Misra S, Bhaisora KS, Mehrotra A, Jaiswal AK, Kumar R. Potential and Pitfalls of Postoperative Volumetric Assessment of Extent of Resection in High-Grade Glioma in Resource-Constrained Settings. Neurol India 2024;72:756-62.
12. Kumar Suman A, Bhattacharjee S, Uppin MS, Fathima ST. Clinicohistoradiological and surgical outcome in diffuse midline glioma. Childs Nerv Syst 2024;40:65-71.
13. Yang X, Hu C, Xing Z, Lin Y, Su Y, Wang X, Cao D. Prediction of Ki-67 labeling index, ATRX mutation, and MGMT promoter methylation status in IDH-mutant astrocytoma by morphological MRI, SWI, DWI, and DSC-PWI. Eur Radiol 2023;33:7003-14.
14. Du N, Zhou X, Mao R, Shu W, Xiao L, Ye Y, Xu X, Shen Y, Lin G, Fang X, Li S. Preoperative and Noninvasive Prediction of Gliomas Histopathological Grades and IDH Molecular Types Using Multiple MRI Characteristics. Front Oncol 2022;12:873839.
15. Nie T, Feng M, Yang K, Guo X, Yuan Z, Zhang Z, Yan G. Correlation between dynamic contrast-enhanced MRI characteristics and apparent diffusion coefficient with Ki-67-positive expression in non-mass enhancement of breast cancer. Sci Rep 2023;13:21451.
16. Marrale M, Collura G, Brai M, Toschi N, Midiri F, La Tona G, Lo Casto A, Gagliardo C. Physics, Techniques and Review of Neuroradiological Applications of Diffusion Kurtosis Imaging (DKI). Clin Neuroradiol 2016;26:391-403.
17. Taha HT, Chad JA, Chen JJ. DKI enhances the sensitivity and interpretability of age-related DTI patterns in the white matter of UK biobank participants. Neurobiol Aging 2022;115:39-49.
18. Pang H, Dang X, Ren Y, Yao Z, Shen Y, Feng X, Wang Z. DKI can distinguish high-grade gliomas from IDH1-mutant low-grade gliomas and correlate with their different nuclear-to-cytoplasm ratio: a localized biopsy-based study. Eur Radiol 2024;34:7539-51.
19. Liu Y, Wang P, Wang S, Zhang H, Song Y, Yan X, Gao Y. Heterogeneity matching and IDH prediction in adult-type diffuse gliomas: a DKI-based habitat analysis. Front Oncol 2023;13:1202170.
20. Gao A, Zhang H, Yan X, Wang S, Chen Q, Gao E, Qi J, Bai J, Zhang Y, Cheng J. Whole-Tumor Histogram Analysis of Multiple Diffusion Metrics for Glioma Genotyping. Radiology 2022;302:652-61.
21. Zhang K, Dai Y, Liu Y, Tao J, Pan Z, Xie L, Wang S. Soft tissue sarcoma: IVIM and DKI parameters correlate with Ki-67 labeling index on direct comparison of MRI and histopathological slices. Eur Radiol 2022;32:5659-68.
22. Zhou M, Chen M, Luo M, Chen M, Huang H. Pathological prognostic factors of rectal cancer based on diffusion-weighted imaging, intravoxel incoherent motion, and diffusion kurtosis imaging. Eur Radiol 2025;35:979-88.
23. Zhang J, Jiang J, Zhao L, Zhang J, Shen N, Li S, Guo L, Su C, Jiang R, Zhu W. Survival prediction of high-grade glioma patients with diffusion kurtosis imaging. Am J Transl Res 2019;11:3680-8.
24. Kahng JY, Kang BH, Lee ST, Choi SH, Kim TM, Park CK, Won JK, Park SH, Son J, Lee JH. Clinicogenetic characteristics and the effect of radiation on the neural stem cell niche in subventricular zone-contacting glioblastoma. Radiother Oncol 2023;186:109800.
25. Zhao X, Ren X, Li M, Jiang H, Li M, Wan H, Zhang Y, Lin S, Zhou D. Subventricular zone-associated classification in isocitrate dehydrogenase-wildtype glioblastomas: improved prognostic value through integration of FLAIR with contrast-enhanced imaging. J Neurosurg 2024;141:1304-13.
26. Xie Z, Suo S, Zhang W, Zhang Q, Dai Y, Song Y, Li X, Zhou Y. Prediction of high Ki-67 proliferation index of gastrointestinal stromal tumors based on CT at non-

contrast-enhanced and different contrast-enhanced phases. Eur Radiol 2024;34:2223-32.
27. Huang Z, Zhou P, Li S, Li K. Prediction of the Ki-67 marker index in hepatocellular carcinoma based on Dynamic Contrast-Enhanced Ultrasonography with Sonazoid. Insights Imaging 2022;13:199.
28. Hokkoku D, Sasaki K, Kobayashi S, Iwagami Y, Yamada D, Tomimaru Y, Asaoka T, Noda T, Takahashi H, Shimizu J, Doki Y, Eguchi H. Apparent diffusion coefficient in intrahepatic cholangiocarcinoma diffusion-weighted magnetic resonance imaging noninvasively predicts Ki-67 expression. Hepatol Res 2024;54:678-84.
29. Torun BC, Sobutay E, Akbulut OE, Saglam S, Yilmaz S, Yonemura Y, Canbay E. Important Predictive Factors for the Prognosis of Patients With Peritoneal Metastasis of Gastric Cancer. Ann Surg Oncol 2024;31:5975-83.
30. Yao R, Cheng A, Zhang Z, Jin B, Yu H. Correlation Between Apparent Diffusion Coefficient and the Ki-67 Proliferation Index in Grading Pediatric Glioma. J Comput Assist Tomogr 2023;47:322-8.
31. Chowdhury R, Alsayegh R, Forest VI, Pusztaszeri MP, da Silva SD, Florianova L, Payne RJ. Ki-67 Labelling Index as a Predictor of Invasive Features in Thyroid Cancer: Retrospective Analysis and Implications. Curr Oncol 2024;31:4030-7.
32. Yuan Q, Zuo FX, Cai HQ, Qian HP, Wan JH. Identifying Differential Expression Genes and Prognostic Signature Based on Subventricular Zone Involved Glioblastoma. Front Genet 2022;13:912227.
33. Sipos TC, Kövecsi A, Kocsis L, Nagy-Bota M, Pap Z. Evaluation of Microvascular Density in Glioblastomas in Relation to p53 and Ki67 Immunoexpression. Int J Mol Sci 2024;25:6810.
34. Zhu Z, Shen J, Liang X, Zhou J, Liang J, Ni L, Wang H, Ye M, Chen S, Yang H, Chen Q, Li X, Zhang W, Lu J, Ge D, Fu L, Zhu Y, Zhang X, Sun Y, Zhang B. Radiomics for predicting grades, isocitrate dehydrogenase mutation, and oxygen 6-methylguanine-DNA methyltransferase promoter methylation of adult diffuse gliomas: combination of structural MRI, apparent diffusion coefficient, and susceptibility-weighted imaging. Quant Imaging Med Surg 2024;14:9276-89.
35. Bai L, Jiang J, Zhou J. Assessment of Ki-67 expression levels in IDH-wildtype glioblastoma using logistic regression modelling of VASARI features. Neurosurg Rev 2023;47:20.
36. Cui Y, Wang X, Wang Y, Meng N, Wu Y, Shen Y, Roberts N, Bai Y, Song X, Shen G, Guo Y, Guo J, Wang M. Restriction Spectrum Imaging and Diffusion Kurtosis Imaging for Assessing Proliferation Status in Rectal Carcinoma. Acad Radiol 2025;32:201-9.
37. Yuan L, Lin X, Zhao P, Ma H, Duan S, Sun S. Correlations between DKI and DWI with Ki-67 in gastric adenocarcinoma. Acta Radiol 2023;64:1792-8.
38. Sun Y, Yang Z, Deng K, Geng Y, Hu X, Song Y, Jiang R. Histogram analysis of quantitative susceptibility mapping and apparent diffusion coefficient for identifying isocitrate dehydrogenase genotypes and tumor subtypes of adult-type diffuse gliomas. Quant Imaging Med Surg 2023;13:8681-93.
39. Granata V, Fusco R, Belli A, Danti G, Bicci E, Cutolo C, Petrillo A, Izzo F. Diffusion weighted imaging and diffusion kurtosis imaging in abdominal oncological setting: why and when. Infect Agent Cancer 2022;17:25.
40. He Y, Chen H, Zhang H, Grimm R, Zhao C, Guo X, Liu Y, Yuan Z. Optimization of scan parameters to reduce acquisition time for RESOLVE-based diffusion kurtosis imaging (DKI) in nasopharyngeal carcinoma (NPC). Br J Radiol 2022;95:20210641.
41. Chiang CW, Lin SY, Cho KH, Wu KJ, Wang Y, Kuo LW. Effects of signal averaging, gradient encoding scheme, and spatial resolution on diffusion kurtosis imaging: An empirical study using 7T MRI. J Magn Reson Imaging 2019;50:1593-603.
42. Su C, Chen X, Liu C, Li S, Jiang J, Qin Y, Zhang S. T2-FLAIR, DWI and DKI radiomics satisfactorily predicts histological grade and Ki-67 proliferation index in gliomas. Am J Transl Res 2021;13:9182-94.
43. Zhu X, He Y, Wang M, Shu Y, Lai X, Gan C, Liu L. Intratumoral and Peritumoral Multiparametric MRI-Based Radiomics Signature for Preoperative Prediction of Ki-67 Proliferation Status in Glioblastoma: A Two-Center Study. Acad Radiol 2024;31:1560-71.

Cite this article as: Wang P, Huang H, Yang L, Chen G. The value of morphological magnetic resonance imaging features combined with diffusion kurtosis imaging for predicting Ki-67 expression levels in high-grade gliomas. Quant Imaging Med Surg 2025;15(4):2813-2826. doi: 10.21037/qims-24-2035